The Vertical Structure of Turbulent Dissipation in Shelf Seas

John H. Simpson

University of Wales, Bangor, School of Ocean Sciences, Menai Bridge, Gwynedd, United Kingdom

William R. Crawford

Institute of Ocean Sciences, Sidney, British Columbia, Canada

Tom P. Rippeth, Andrew R. Campbell, and Joseph V. S. Cheok

University of Wales, Bangor, School of Ocean Sciences, Menai Bridge, Gwynedd, United Kingdom

(Manuscript received 28 March 1995, in final form 24 January 1996)

ABSTRACT

The free-fall FLY profiler has been used to determine the variation in energy dissipation ϵ in the water column over a tidal cycle at mixed and stratified sites in the Irish Sea. It was found that ϵ exhibits a strong M_4 variation with a pronounced phase lag that increases with height above the bed. In mixed conditions this M_4 signal, which extends throughout the water column, is reasonably well reproduced by turbulent closure models of the vertical exchange. In the summer stratified situation, the M_4 signal in ϵ is confined to about 40 m above the seabed with phase delays of more than 4 h relative to the seabed. The lowest levels of dissipation ($\sim 10^{-5}$ W m^{-3}), measured in the pycnocline, are significantly above the system noise level and much higher than predicted by a model using the Mellor–Yamada level 2 closure scheme (MY2.0). However, when allowance is made for the diffusion of TKE, the model (MY2.2) simulates the depth–time distribution of dissipation in the stratified case satisfactorily if the diffusivity $K_q = 0.2ql$. With K_q set equal to vertical eddy viscosity N_z, which depends on the Richardson number Ri, the model underestimates dissipation in the pycnocline by two decades, which would imply the possibility of a midwater source of TKE. The observed depth-integrated dissipation is found to be consistent with estimates based on the energy lost from the tidal wave when adjustment is made for the unsampled high energy region close to the bed.

1. Introduction

A central part of the current agenda in physical oceanography of shelf seas is to understand the interactions of the processes that control vertical structure and the diffusion of properties through the water column. First-order accounts of the evolution of the density structure have been given in terms of "prescriptive models" based on energy arguments and simplified assumptions about the efficiency of mixing processes (e.g., Simpson and Bowers 1984) and, for the case of freshwater buoyancy input, on prescribed forms of the velocity structure (e.g., Simpson et al. 1991). Such models do not deal with the dynamics of tidal and density-driven flow explicitly, but rely on combining separate analytical solutions for each component of the flow.

To achieve a more fundamental description of the processes involved and to allow for the nonlinear interaction between them, it is necessary to solve the dynamical equations for appropriate forcing by the tides, specified as components of the surface slope, and surface wind stress. In order to allow for the crucial interaction between vertical fluxes and water column stratification, the solution must be completed by an appropriate closure scheme, several of which are currently in use (e.g., Luyten et al. 1996). Most of these schemes involve the explicit representation of the turbulent kinetic energy and its dissipation function ϵ through which energy is converted into heat. It is clear that a critical test of models based on these schemes should be their ability to describe the depth dependence and time evolution of the turbulent parameters. Satisfactory performance of a closure scheme in such 1D tests would seem to be a necessary prerequisite for its utilization in 3D models.

Until recently it was only possible to test model performance against mean flow parameters in circumstances of high shear (Davies and Flather 1987). In these conditions differences in the profile of vertical velocity can be effective in discriminating between the schemes. However, in many cases of tidally dominated flow, the velocity profile is insensitive to changes in the

Corresponding author address: Prof. John H. Simpson, School of Ocean Sciences, University of Wales, Bangor, Menai Bridge, Gwynedd LL59 5EY, United Kingdom.

form of eddy viscosity profile. The only significant changes are in regions close to the boundaries and so are not readily accessible to measurement. The consequence is that it is not generally possible to confidently predict vertical mixing coefficients with the accuracy required in models of water column processes. An alternative and, we might hope, a more revealing strategy is to test the models more directly and fundamentally at the "intermediate" level by comparing measurable aspects of the turbulence with model simulations. In this contribution, we report on the implementation of this strategy using a set of observations of turbulent dissipation through the water column in three contrasting tidal flow regimes in the European shelf seas.

2. A 1D model of vertical structure and flow

The flow properties, both mean and turbulent, are to be compared with hindcasts of the flow made using point models of the dynamics and vertical diffusion with different closure schemes. Initially we shall use the 1D dynamics model (Simpson and Sharples 1992) with a Mellor–Yamada level 2 closure scheme, arguably the simplest type of scheme needed in order represent the interaction of flow and stratification. The model uses an explicit scheme to integrate the equations of motion for the velocity components u and v:

$$\frac{\partial u}{\partial t} = -\frac{1}{\rho}\frac{\partial P}{\partial x} + fv + \frac{\partial}{\partial z}\left(N_z \frac{\partial u}{\partial z}\right) \qquad (1)$$

$$\frac{\partial v}{\partial t} = -\frac{1}{\rho}\frac{\partial P}{\partial y} - fu + \frac{\partial}{\partial z}\left(N_z \frac{\partial v}{\partial z}\right), \qquad (2)$$

where N_z is the vertical eddy viscosity and z increases positively from the seabed. The bottom boundary condition is a quadratic stress law; wind stress at the sea surface is also given in terms of a quadratic drag prescription using observed hourly wind vector data.

The horizontal pressure gradient terms in Eqs. (1) and (2) are given by

$$\frac{1}{\rho}\frac{\partial P}{\partial x} = g\left(\frac{\partial \eta}{\partial x}\right)_{\text{tidal}} + g\left(\frac{\partial \bar{\eta}}{\partial x}\right)_{\text{nontidal}} + g(h - z)\frac{\partial \rho}{\partial x} \qquad (3)$$

and similarly for the y component. The first term on the right of Eq. (3) is an oscillating sea surface slope that provides the tidal forcing. It is derived from a 2D vertically integrated model (Proctor and Smith 1991), which covers the entire European shelf with a resolution of about 12 km. The second term represents a mean surface slope, which may be required to represent steady, or slowly varying nontidal flows. The effect of horizontal density gradients is represented in the final term that is generally small in the present context where such gradients are weak. Consequently we need con-

sider only the vertical diffusion of heat and salt in the advection–diffusion equation, which takes the form:

$$\frac{\partial(s, T)}{\partial t} = \frac{\partial}{\partial z}\left(K_z \frac{\partial(s, T)}{\partial z}\right), \qquad (4)$$

where K_z is the vertical eddy diffusivity. There is no flux of salt or heat through the seabed, and no net flux of salt at the surface. Surface heating is specified in terms of global solar radiation, dewpoint temperature, and wind speed (following Simpson and Bowers 1984)—the values of which are observations from nearby meteorological stations.

A level-2 turbulence closure scheme is used to calculate vertical profiles of N_z and K_z as functions of local stability (Mellor and Yamada 1974), via

$$N_z = S_M lq; \quad K_z = S_H lq, \qquad (5)$$

where S_M and S_H are stability functions of the local gradient Richardson number, and l is a prescribed length scale given by

$$l = \kappa z\left(1 - \frac{z}{h}\right)^{1/2}, \qquad (6)$$

where z is the height above the bed and κ is von Kármán's constant.

The evolution of the turbulent kinetic energy $(q^2/2)$ is described by the equation (Tennekes and Lumley 1972)

$$\frac{\partial}{\partial t}\left(\frac{q^2}{2}\right) - \frac{\partial}{\partial z}\left(K_q \frac{\partial}{\partial z}\left(\frac{q^2}{2}\right)\right)$$

$$= N_z\left[\left(\frac{\partial u}{\partial z}\right)^2 + \left(\frac{\partial v}{\partial z}\right)^2\right] + K_z\left(\frac{g}{\rho}\frac{\partial \rho}{\partial z}\right) - \frac{q^3}{B_1 l}. \qquad (7)$$

The second term on the lhs represents the effects of vertical diffusion while the three terms on the rhs are respectively shear production, work against buoyancy forces and energy dissipation involving the Mellor–Yamada constant $B_1 = 15$.

We shall utilize three versions of the model: In the simplest (MY level 2.0), we neglect the time derivative and vertical diffusion terms on the left-hand side of Eq. (7), and assume a local equilibrium between shear and buoyancy production of turbulent KE and dissipation. In the other two versions (MY2.2), we shall retain the left-hand side of Eq. (7) and hence allow for the influence of turbulence diffusing upward into the flow from the main generation zone near the bottom boundary with either $K_q = N_z = S_M ql$ (MY2.2A) or the simple form $K_q = 0.2ql$ (MY2.2B) in which the diffusion is independent of the stability functions (Deleersnijder and Luyten 1994).

For each of the observational periods and locations, we have run the model with forcing by tidal slopes from

a 2D model, the observed winds, and surface heat exchange variables.

3. Measurement of turbulent dissipation

The observations, over one or two tidal cycles, were made at three sites in the Irish Sea (Fig. 1) during March and July 1993. The two strongly mixed sites M1 and M3 were the focus of the March campaign, while in July contrasting observations were made at the low energy site S1 where strong seasonal stratification prevailed. The sites selected were in regions of horizontally uniform conditions with weak density gradients $(<3 \times 10^{-6} \text{ kg m}^{-4})$. The measurements at the mixed sites M1 and M3 were taken close to the vernal equinox when the surface buoyancy flux is minimal. At M1 in March and S1 in July, the observations were made in parallel with measurements from conventional moored current meters. Each sequence of dissipation profiles was followed by measurements with a profiling CTD/transmissometer system.

The measurements of dissipation were made using the FLY profiler (Dewey et al. 1987), which is equipped with a guard ring that allows measurements to be made to within 15 cm of the seabed. The measurements thus cover almost the entire water column except for a near-surface region (about 5 m thick) in which turbulence from the ship's wake may corrupt the results. The profiler falls freely at a speed of 0.70–0.80 m s^{-1} and measures components of the horizontal velocity via a piezoelectric sensor, which detects the force exerted on a small aerofoil probe by the transverse flow. This force, which is proportional to the horizontal velocity, is differentiated to give the vertical shear on scales down to ~ 1.5 cm. Estimates of dissipation are derived from the mean square shear using the relationship for isotropic turbulence

$$\epsilon = 7.5\mu\overline{\left(\frac{\partial u}{\partial z}\right)^2},$$ (8)

where μ is the dynamic viscosity of seawater and dissipation is given in units of watts per cubic meter. The mean-square shear is calculated by first deriving the power spectrum for each section of the record (depth
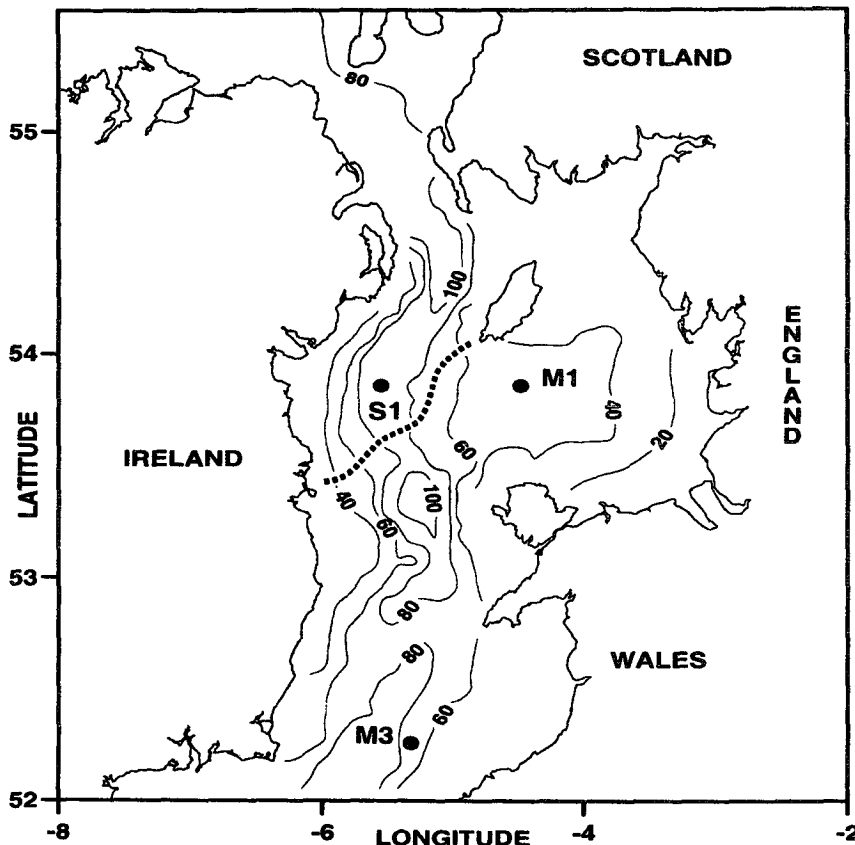

Fig. 1. Location of measurement sites in the Irish Sea. M1 mixed regime: depth, $h = 60$ m, M_2 tidal current amplitude, $U_2 = 0.7$ m s^{-1}; M3 mixed regime: $h = 90$ m, $U_2 = 0.8$ m s^{-1}; S1 stratified regime: $h = 90$ m, $U_2 = 0.3$ m s^{-1}. The principal tidal mixing front separating mixed and stratified regions is shown as a dashed curve.
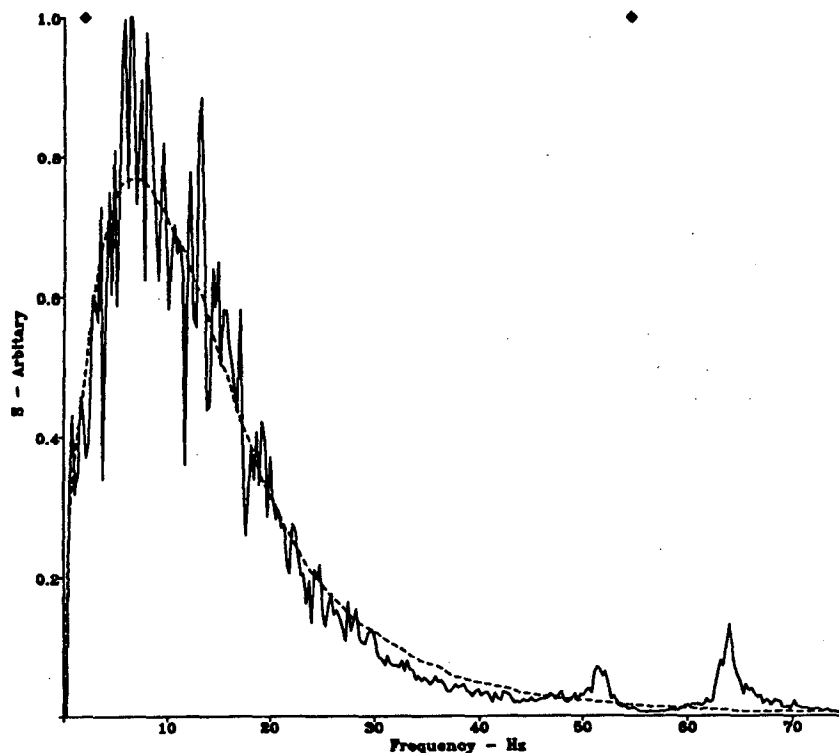
FIG. 2. Power spectrum $S(w)$ of dissipation. The solid line shows an average power spectrum for 25 power spectra measured with $\epsilon \sim 10^{-4}$ W m^{-3}. The diamonds indicate the integration limits and the dashed line the spectral fit (from Nasmyth 1970) used to extrapolate the dissipation outside the limits of integration.

interval $= 1.5$ m). This allows the elimination of high-frequency noise and the application of a spectral correction for the rolloff of the shear probe response. The latter is obtained by matching the total energy between high and low frequency cutoff points to a form of the Kolmogorov spectrum (Nasmyth 1970) as in Fig. 2. The upper frequency limit is normally set to 55 Hz (wavenumbers $k_1 \sim 494$ m^{-1}) at which point the sensor response is reduced by 50%. For dissipation rates lower than 10^{-4} W m^{-3}, however, this limit has been reduced to avoid unnecessary noise contamination of the spectrum.

A spectral correction is also used to correct for dissipation at frequencies lower than the 2 Hz ($k_2 \sim 18$ m^{-1}) cutoff. This cutoff is applied as the signal may be contaminated by low-frequency wobble of the profiler body and energy "leakage" from the mean flow. These spectral corrections generally represent a small percentage of the observed dissipation and exceeded 20% only at high dissipations ($>10^{-2}$ W m^{-3}) in the near-bed region.

After impact with the bottom, the profiler is hauled back to the surface by a light Kevlar tether, which also acts as a transmission cable for the data stream. The profiler is operated in a yo-yo mode, cycling between surface and bottom while the ship moves ahead at 0.5 knots. During descent the tether line is fed out by a

spooler winch to ensure that the free-fall of the profiler is not impeded. A sequence of up to ten profiles were taken between hourly CTD profiles over one or two semidiurnal tidal cycles.

4. Results

a. The mixed regimes (M1 & M3)

After spectral correction, the sequences of dissipation profiles have been combined into plots showing the evolution of dissipation over the tidal cycle. Figure 3a illustrates the results for measurements over a 25-hour period, in the form of $\log_{10}\epsilon$, at the energetic mixed site M1 where the mean depth is 60 m and the surface tidal stream had an amplitude of about 1 m s^{-1}. Dissipation generally decreases with height by three orders of magnitude from peak values of $\epsilon = 0.1$ W m^{-3} close to the bed. At all levels the intensity of the dissipation is clearly related to the phase of the current so that there is a marked quarter-diurnal variation in ϵ with a phase lag that increases with height.

Similar patterns of variation with height and time are apparent in Fig. 4a for the other mixed station (M3). The water column is deeper and tidal currents were weaker at this station. As a consequence, dissipation
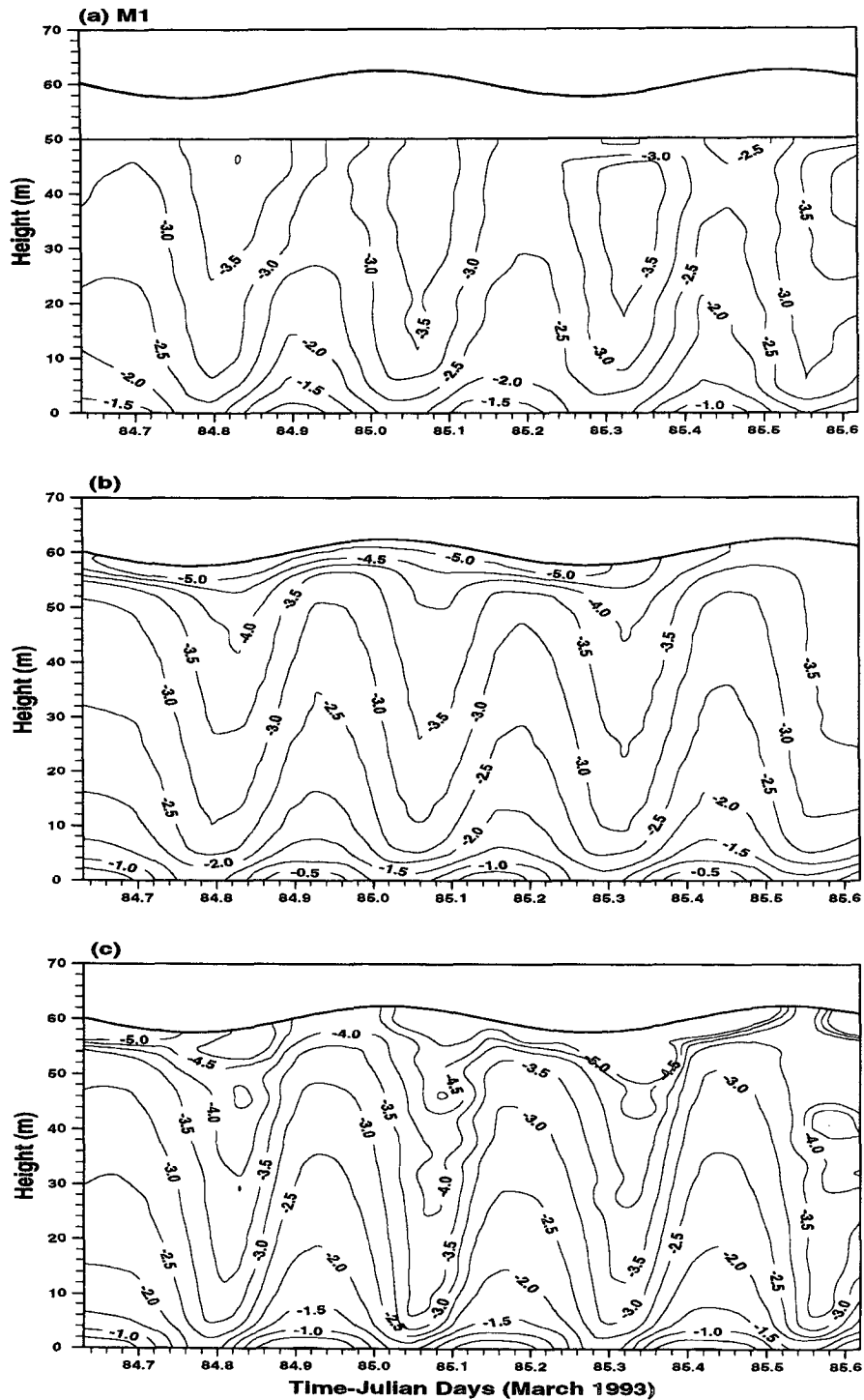
FIG. 3. $\log_{10}\epsilon$ (W m^{-3}) distribution over two tidal cycles at the mixed site M1 from (a) the FLY profiler observations, (b) the model simulation using MY2.2A, and (c) the model simulation using MY2.0. There is no observational data for ϵ within 5 m of the sea surface because of contamination by turbulence from the ship's wake.

levels are somewhat lower and the phase lag is more pronounced.

For both cases we show the corresponding model simulations (Figs. 3b,c and 4b,c) obtained using the MY2.0 and MY2.2A schemes. These predictions have been made without tuning of the MY parameters (from Simpson and Sharples 1992) and using the tidal forcing directly from the 2D model without adjustment. The
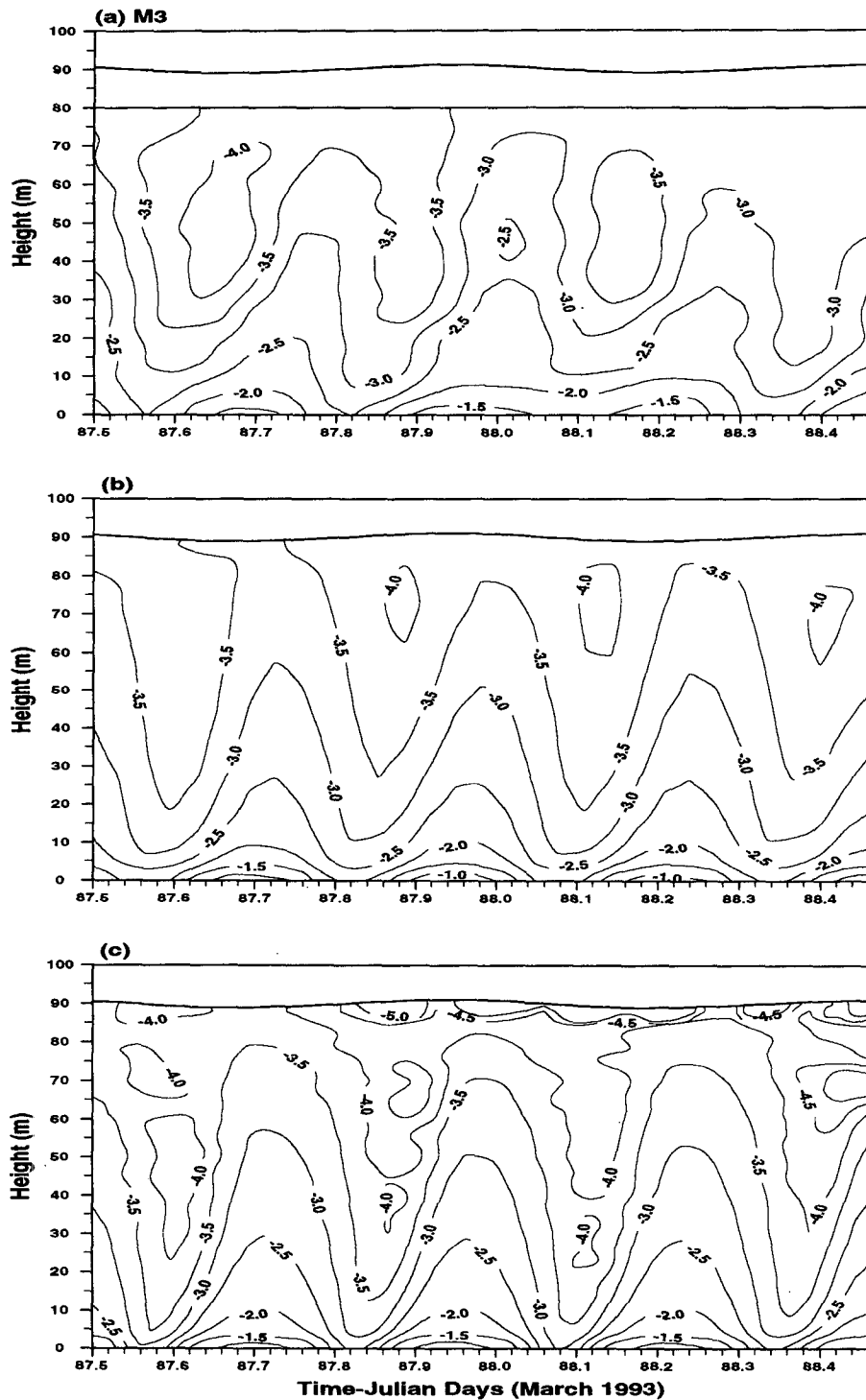

FIG. 4. $\log_{10}\epsilon$ (W m^{-3}) distribution over two tidal cycles at the mixed site M3: layout as in Fig. 3.

models reproduce all the main features of the observed ϵ distributions, for the two mixed cases, although the fit is apparently somewhat better for the MY2.2 version. The models also give a reasonable account of the mean currents measured at the adjacent current meter moorings (see Fig. 5). A small asymmetry between the ebb and flood half cycles in this case is associated with a nontidal northward residual of magnitude 0.09 m s^{-1}, which is incorporated into the model simulations by means of the mean slope term. This residual component is also responsible for the asymmetry in dissipation between ebb and flood apparent in Figs. 3a–c.

b. The seasonally stratified regime (S1)

The measurements made in July at the stratified site (S1) are presented in Fig. 6. The existence of strong stable stratification is confirmed by the CTD temperature data (Fig. 6a). In this case, with a mean water depth of 90 m and current amplitude of 0.45 m s^{-1}, the energy dissipation levels, Fig. 6b, are correspondingly reduced with peak values near the bed of $\epsilon \sim 3.0 \times 10^{-2}$ W m^{-3}. In midwater there is an extensive region of low dissipation where $\epsilon \sim 1.0 \times 10^{-5}$ W m^{-3}. This corresponds to a level about one and a half decades above the noise level for the FLY measurements (equivalent to a dissipation of 3×10^{-7} W m^{-3}). In contrast to the well-mixed cases, the pronounced quarterdiurnal variation of ϵ, while marked near the bottom boundary, only extends upward to a height of about 40 m above the bed. Within this boundary layer region there is again an increasing delay in the time of maximum dissipation with height above the seabed.

The MY models (Figs. 6c,d) simulate the principal characteristics of the observed behavior in most respects, although the predicted ϵ levels in midwater from MY2.0 are significantly lower than those observed. Adding diffusion in the MY2.2B markedly improves the simulation of the ϵ distribution, especially in the low-energy region between 40 and 80 m above the bed where hindcast levels are now close to those observed.

5. M₄ analysis

We have further examined the time dependence of dissipation in the water column, and the skill of the model schemes, by fitting the data to a quarterdiurnal constituent (M$_4$) of the form:

$$\epsilon = a_0 + a_4 \sin(\omega_4 t - \psi_4), \qquad (9)$$

where a_0 represents the mean dissipation over the tidal cycle and a_4 and ψ_4 are the amplitude and phase lag of the M$_4$ constituent. A least squares procedure is used to fit Eq. (9) to the dissipation time series at each level in the water column and thus determine a_0, a_4, and ψ_4 as functions of height.

Results for the observations at the mixed site M3 (Fig. 7) show the mean a_0 and amplitude a_4 are of

(a) Height @41m

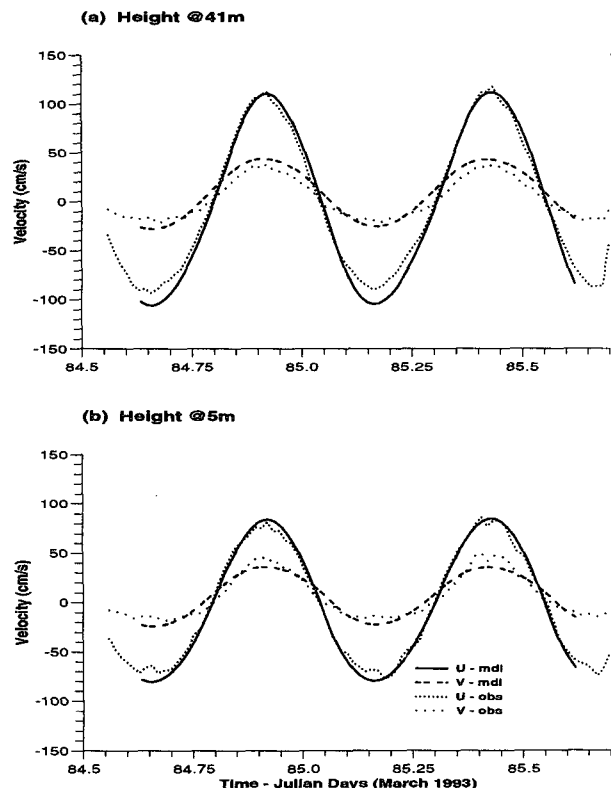(b) Height @5m

Time – Julian Days (March 1993)

FIG. 5. Components of the mean flow over the observational period at M1 from current meter observations and the model MY2.2A at (a) a height of 41 m above the bed and (b) a height of 5 m above the bed. The observed mean flow has been simulated in the model by the application of a steady surface slope.

similar magnitude, with both decreasing by more than two decades between the bed and a height of 60 m. At the same time there is a steady increase in the observed phase lag with maximum delay of about 1.5 h relative to the bed at a height of 70 m. Closely comparable results were obtained for the shallower mixed site M1 where the observed phase lag between the bed and 50-m height is about 1 h. The behavior at both locations is reflected in the model simulations with the vertical structure of mean and oscillating components well represented. The MY2.2 scheme again achieves a rather better overall simulation.

At the seasonally stratified site (Fig. 8), the M$_4$ oscillation diminishes with height and there is a well-defined phase shift increasing from the bed to ~4 h at a height of 40 m. Above this level, the oscillatory component is weak with R^2, the percentage of variance explained, diminishing to near zero and the phase inadequately determined.

While the three versions of the model reproduce the form of depth variation of the mean and oscillatory amplitude in the layer below 40 m, there are marked differences in their performance further up the water
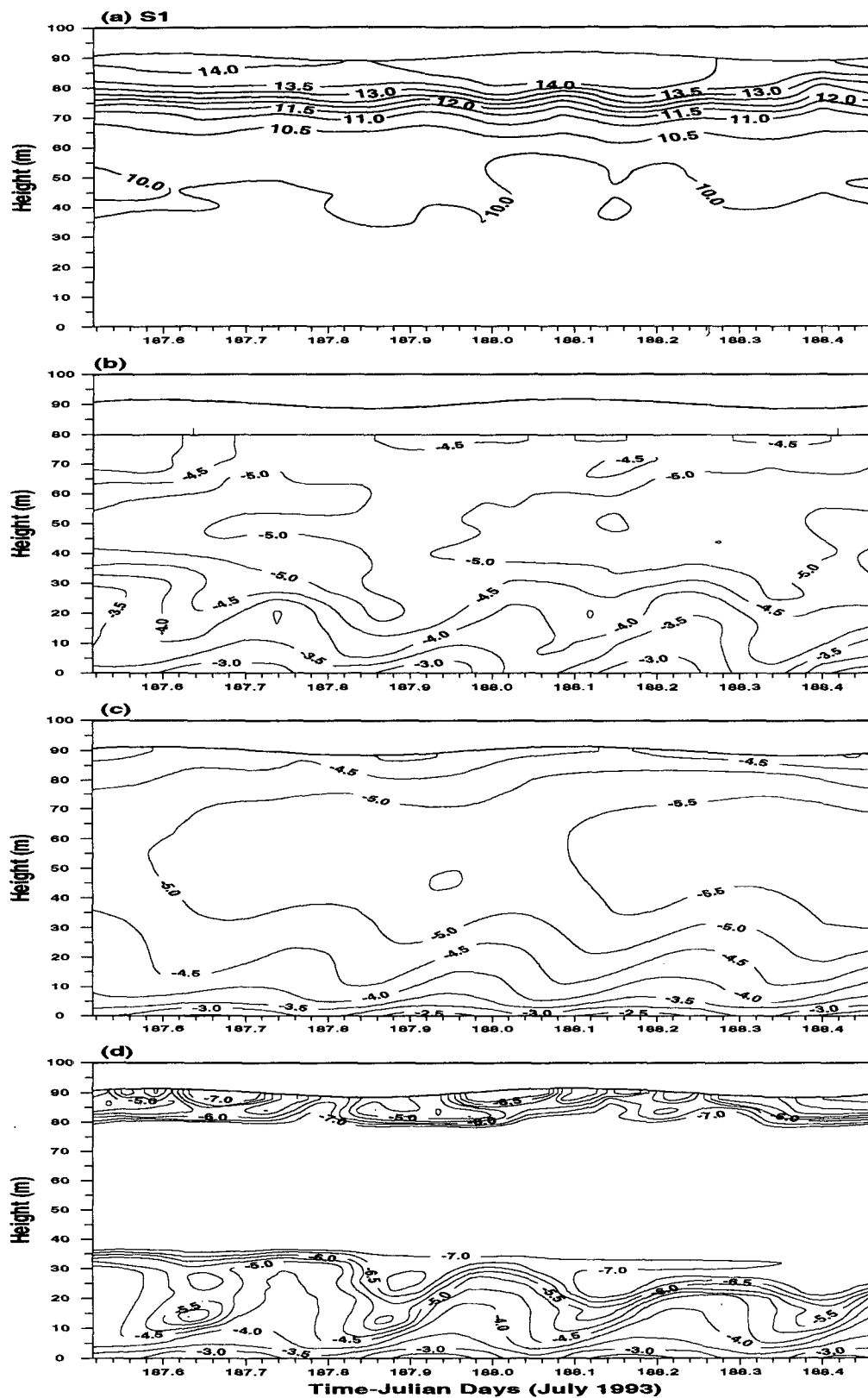
FIG. 6. Observations and model simulations for the stratified site S1: (a) temperature structure (°C) from hourly CTD profiles, (b) observed $\log_{10}\epsilon$ (W m^{-3}) distribution, (c) $\log_{10}\epsilon$ (W m^{-3}) distribution simulated using the model with MY2.2B, and (d) $\log_{10}\epsilon$ (W m^{-3}) distribution simulated using the model with MY2.0.
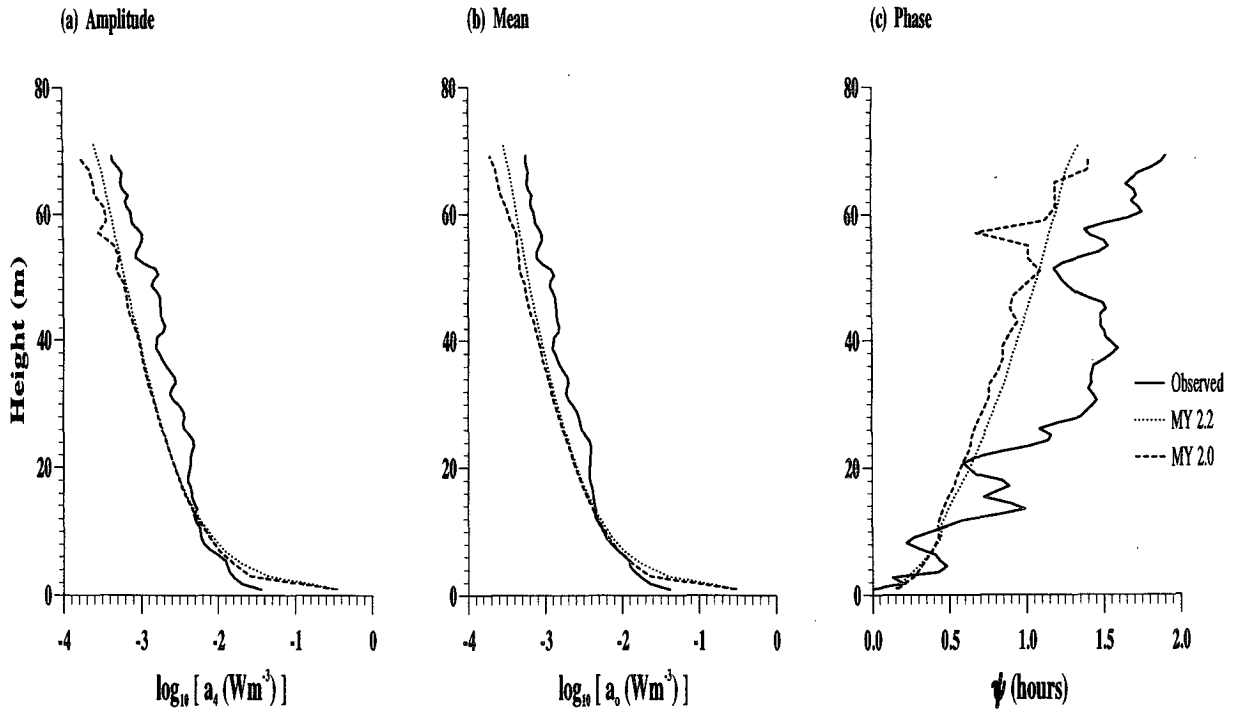
(a) Amplitude   (b) Mean   (c) Phase

FIG. 7. Tidal M_4 analysis at mixed site M3 from observations and models MY2.0 and MY2.2A: (a) Amplitude of the M_4 oscillation a_4, (b) Mean dissipation a_0, (c) Phase lag ψ_4.

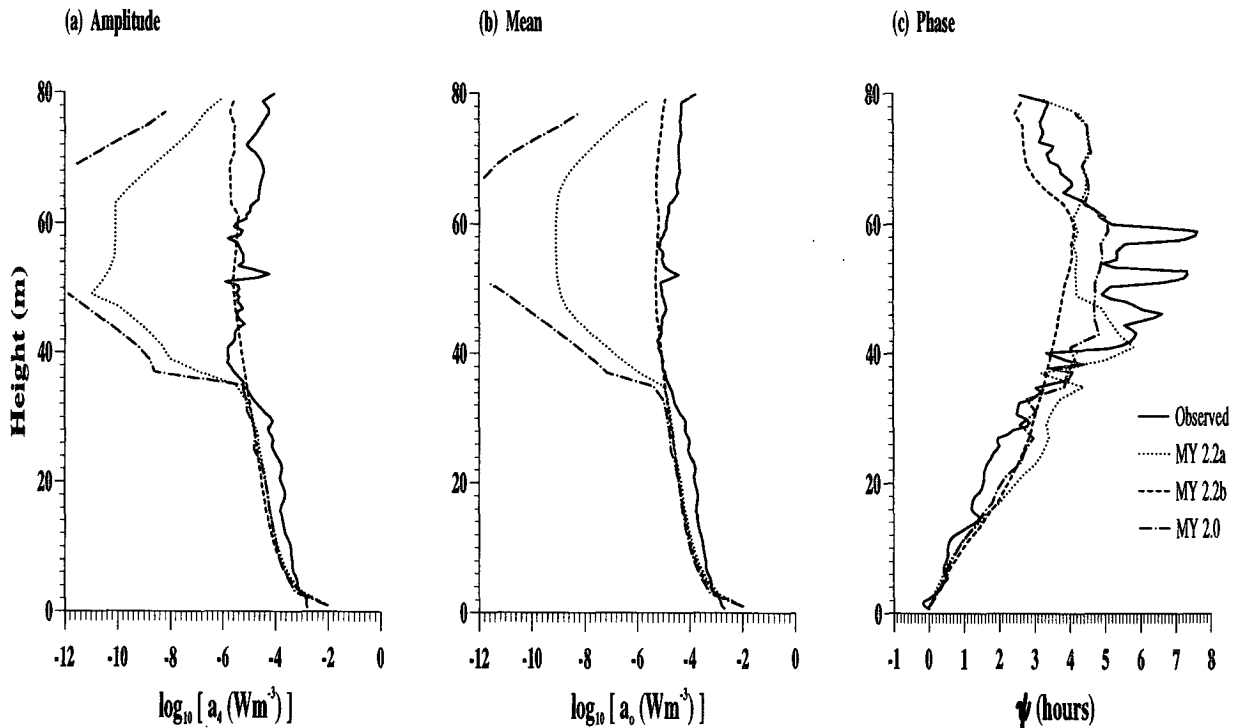(a) Amplitude   (b) Mean   (c) Phase

FIG. 8. As in Fig. 7 but at stratified site S1 from observations and models MY2.0, MY2.2A, and MY2.2B.
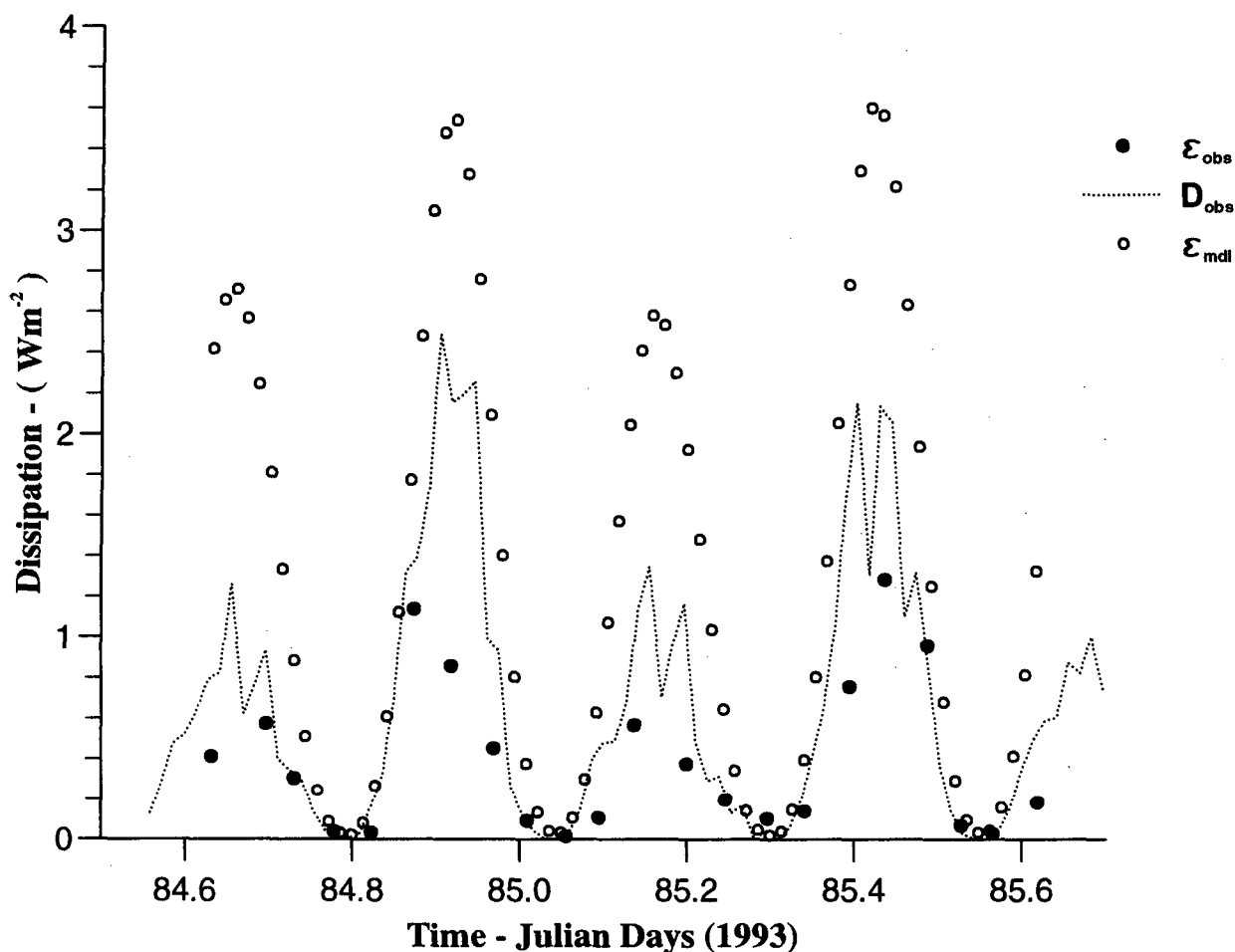
M1 site

FIG. 9. Depth-integrated dissipation, $\int \epsilon dz$, at site M1 from observations (solid circles), model MY2.2A (open circles), and the dissipation calculated using the tidal current measured at 5 m above the bed using Eq. (10) (dotted line).

column. Between 40 and 80 m above the bed, the local equilibrium closure (MY2.0) produces ϵ levels that are many decades lower than those observed. Adding vertical diffusion with $K_q = N_z$ (MY2.2A) improves the situation somewhat but dissipation is still seriously underestimated. When, however, the model is implemented with $K_q = 0.2ql$ (MY2.2B), ϵ levels in midwater are close to those observed and the general structure of the vertical variation of amplitude and phase are reproduced.

6. Discussion

These measurements of dissipation have revealed, for the first time, the vertical structure and time dependence of ϵ over a tidal cycle for European shelf seas,

and yielded a valuable database for the evaluation of turbulent closure schemes. As a check on the accuracy of the observed dissipation we might compare the dissipation, integrated through the water column, with the total energy loss from the tide, which is known (to first order) from large-scale models of the tide to be

$$D = C_d \rho U^3, \qquad (10)$$

where U is the depth-mean tidal current speed and the drag coefficient C_d has a value of 2.5×10^{-3}. Figure 9 shows a comparison of the depth integral of the local dissipation ϵ with D based on the current speed at 5 m above the bed for measurements at the well-mixed station M1. The two quantities are of similar magnitude and exhibit a comparable semidiurnal cycle but the in-

tegrated dissipation is generally smaller by a factor of 2. We should recall, however, that the ϵ measurements terminate 15 cm from the bed and a high proportion of the production and dissipation of TKE occurs in this region. Using the law of the wall, we can estimate the ratio of the dissipation that occurs in the last 0.15 m to the total for the bottom 10 m as

$$\frac{\ln\left(\frac{10}{0.15}\right)}{\ln\left(\frac{10}{z_0}\right)} = 0.46, \qquad (11)$$

which with $z_0 = 0.1$ cm accounts for much of the discrepancy. In any case, the ϵ measurements are subject to a number of unavoidable uncertainties. Dewey and Crawford (1988) show that the errors in determining the fall speed of the probe (5%) contribute an uncertainty of 20% since $\epsilon \propto w^4$. Other significant error contributions arise from the shear probe calibration (7%), the gain of the differentiator (2%), and the determination of the molecular viscosity (5%). Together the potential errors amount to about 50% of the mean so that closer agreement between the observed integrated dissipation and D would be fortuitous. We also show in Fig. 9 the equivalent integrated dissipation from the model, which matches the time evolution of observations but is generally higher than the measurement although, again, the discrepancy is not large compared with uncertainties in the observations.

A striking feature of the observations in both mixed and stratified conditions is the pronounced phase delay in the M_4 cycle of dissipation with height above the bed. For the mixed situation at M3, delays of up to 2 h, relative to the seabed, in the time of maximum dissipation were observed at a height of 70 m. Even larger phase lags, of up to 4 h, were found to occur in the bottom boundary layer of the stratified situation. The magnitude and height dependence of these phase lags is reasonably well described by all forms of the models, including the MY2.0 version which does not include vertical diffusion. The inference must clearly be that the phase lag is primarily a result of a progressive delay in the phase of the production term with only a small contribution from the effects of diffusion.

In most respects the models give a fair account of the observed depth–time distributions of ϵ under mixed conditions. The magnitude and distribution of dissipation are well reproduced, at least on a log scale, and the flood–ebb asymmetry at M1 is accounted for when a small residual current is included. The incorporation of diffusion in the MY2.2 schemes brings about a small but significant improvement over the local equilibrium model (MY2.0). For the stratified situation, the results of the different schemes are more divergent. Both versions with diffusion (MY2.2A and B) represent an improvement on the local equilibrium closure, but for

MY2.2A in which $K_q = N_z$ depends directly on stratification, there is a failure to predict the correct level of dissipation in the strongly stratified portion of the water column. Between 40 and 80 m above the bed, observed values do not fall below 10^{-5} W m^{-3}, which is a factor of 30 above the estimated noise level of the FLY system, while the MY2.2A model hindcasts are several orders of magnitude lower. The implication would seem to be that there is a local midwater source of TKE, which is not represented in the models. On the other hand, employing the widely used form $K_q = 0.2ql$ (MY2.2B), diffusion of turbulence into the interior of the water column is increased and the model hindcasts the vertical structure rather well without an appeal to additional TKE sources.

Two rather different interpretations of the ϵ distributions remain. Using the physically reasonable MY2.2A, in which TKE diffuses in the same way as the mean momentum, we must conclude that there is a midwater source of turbulent kinetic energy. At this stage we have no firm indication of the source of this additional energy input, but it may be associated with the frequently alleged stirring by the internal tide and internal waves or it may arise from dissipation of inertial motions generated in the surface layers by wind stress.

In the alternative interpretation, turbulence is allowed to diffuse more efficiently, as in MY2.2B, so that there is no need for additional inputs. The difficult question however, remains of how we justify the use of the simple form $K_q = 0.2ql$ in stratified conditions when we would expect control to be exerted by the Richardson number.

REFERENCES

Davies, A. M., and R. A. Flather, 1987: Computing extreme meteorologically induced currents, with application to the north-west European continental shelf. *Contin. Shelf Res.,* **7**, 643–683.

Deleersnijder, E., and P. Luyten, 1994: On the practical advantages of the quasi-equilibrium version of the Mellor and Yamada level 2.5 closure applied to marine modelling. *Appl. Math. Modelling,* **18**, 281–287.

Dewey, R. K., and W. R. Crawford, 1988: Bottom stress estimates from vertical dissipation rate profiles on the Continental Shelf. *J. Phys. Oceanogr.,* **18**, 1167–1177.

——, ——, A. E. Gargett, and N. S. Oakey, 1987: A microstructure instrument for profiling oceanic turbulence in coastal

bottom boundary layers. *J. Atmos. Oceanic Technol.,* **4,** 288–297.

Lutyen, P. J., E. Deleersnijder, J. Ozer, and K. G. Ruddick, 1996: Presentation of a family of turbulence closure models of stratified shallow water flows and application to the Rhine outflow region. *Contin. Shelf Res.,* **16,** 101–130.

Mellor, G. L., and T. Yamada, 1974: A hierarchy of turbulence closure models for planetary boundary layers. *J. Atmos. Sci.,* **31,** 1791–1806.

Nasmyth, P. W., 1970: Oceanic turbulence. Ph.D. thesis, University of British Columbia, 105 pp.

Proctor, R., and J. A. Smith, 1991: The depth averaged residual circulation on the North West European Shelf. Proudman Oceanographic Laboratory Rep. 20, 255 pp. [Available from Bidston Observatory, Birkenhead, Merseyside L43 7RA, United Kingdom.]

Simpson, J. H., and D. G. Bowers, 1984: The role of tidal stirring in controlling the seasonal heat cycle in shelf seas. *Ann. Geophys.,* **2,** 411–416.

——, and J. Sharples, 1992: Dynamically active models in the prediction of estuarine stratification. *Dynamics and Exchanges in Estuaries and the Coastal Zone,* D. Prandle, Ed., Amer. Geophys. Union, 101–113.

——, ——, and T. P. Rippeth, 1991: A prescriptive model of stratification induced by freshwater run-off. *Estuar. Coastal Shelf Sci.,* **33,** 23–35.

Tennekes, H., and J. L. Lumley, 1972: *A First Course in Turbulence.* The MIT Press, 300 pp.